JOURNAL OF CATALYSIS **168,** 511–521 (1997)
ARTICLE NO. CA971697

Spectroscopic Characterization of Dealuminated H-Mordenites: The Role of Different Aluminum Species on the SCR of NO with Methane

M. Lezcano,* A. Ribotta,* E. Miró,* E. Lombardo,*,[1] J. Petunchi,* C. Moreaux,† and J. M. Dereppe†

*Instituto de Investigaciones en Catálisis y Petroquímica, INCAPE (FIQ,UNL-CONICET), Santiago del Estero 2829, 3000 Santa Fe, Argentina; and †Laboratoire de Chimie-Physique, Université Catholique de Louvain, Pl. L. Pasteur 1-Bte 3A, 1348 Louvain-la-Neuve, Belgium

Received November 25, 1996; revised February 28, 1997; accepted March 14, 1997

In order to understand the role of different aluminum species in the selective catalytic reduction of nitrogen oxides with methane over H-mordenites, solids with varying Si/Al ratios (5.9–16.9) were prepared by acid leaching. They were thoroughly characterized before and after reaction. The distribution of Al was determined through ^{27}Al MAS NMR. All the samples presented three signals, one at 54 ppm corresponding to lattice Al^{IV}, another at 0 ppm associated with octahedrally coordinated Al, and a broad band, BB (ca 100 ppm wide), assigned to aluminum containing species. As the spinning rate increased up to 11.3 kHz, a decrease of the BB intensity and an increase of the Al^{IV} signal took place, while the Al^{VI} slightly increased. The best estimate of lattice aluminum was obtained from the Al^{IV} peak intensity. Despite the high spinning rate employed, it was possible to observe only between 70–80% of the total Al present in the samples. The catalysts were also analyzed by XRD, FTIR, and ^{129}Xe NMR of physisorbed Xenon. By correlating the variation of the *a* cell constant with Al/u.c., only qualitative information was obtained. The IR band shift at ca 572 and 588 cm^{-1} at higher wave lengths, and the decrease of the bands intensity at 650 and 730 cm^{-1} with decreasing Al content were examined. These changes in the IR spectra are a clear indication of the dealumination process carried out in the samples, thus supplementing the ^{27}Al MAS NMR results and supplying information on the dealumination mechanism as well. ^{129}Xe NMR results shows that nonlattice aluminum may interrupt the free exchange of molecules between the main channels and side pockets. The turnover frequency of NO disappearance remains constant with varying lattice aluminum content. The catalysts were partially deactivated after being on stream at 650°C due to the additional dealumination occurring at high temperatures in the reacting stream. Both in fresh and used catalysts, only the sites related with lattice aluminum were active in the reaction under study. The nonlattice, polymeric species, generated during dealumination hinder the access of the reactant molecules to the active sites.

1. INTRODUCTION

Metal-exchanged zeolites have been widely reported as catalysts for the selective reduction of NO_x with various hydrocarbons in the presence of excess oxygen (1–7). Due to its activity Cu-ZSM5 is among the most studied catalysts (8, 9). However, this solid is not efficient to reduce NO_x when the hydrocarbon is methane. It preferentially catalyzes the methane combustion and no hydrocarbon remains available to reduce NO_x (10). On the other hand, several authors (11–14) reported that H-zeolites are able to reduce NO_x with methane. The relatively low activity of these solids and their lack of stability in the presence of water at high temperatures could make them not commercially feasible (15).

Several studies related with the reaction mechanism have been reported (16–19) and various authors have speculated about the nature of the active sites for this reaction, over different catalysts. However, the deactivation phenomena undergone by H-zeolites have not been thoroughly investigated; most studies in this respect are concerned with Cu-ZSM-5 (9, 20–22). In this regard Grinsted *et al.* (20) and Kung and co-workers (21) pointed out that the deactivation of Cu-zeolites aged in an air stream with 10% H_2O at 410°C and after being in wet reaction stream (NO, C_3H_8, O_2, and H_2O) was due to dealumination of the zeolite framework. This phenomenon was more severe in protonic zeolites according to the results advanced by Lezcano *et al.* (13). Within this framework, the study of H-zeolites can throw light on how dealumination induces catalyst deactivation. Besides, recent contributions have also reported a synergetic effect between metals and the acid function (23, 24). Both of these topics encourage a systematic study of purely acidic catalysts.

During either thermal or acid dealumination, the removal of aluminum from a zeolite network produces significant structural changes and modification of its catalytic properties. In most cases, the extra-framework aluminum remains, at least in part, inside the zeolite channels originating different kinds of aluminum residues.

The dealumination process may be purposely done or may occur during use through combined exposure to heat, water vapor, and/or reactants and products while on stream. Thus, it is essential to use adequate tools to characterize what happens upon dealumination.

[1] E-mail: nfisico@figus.unl.edu.ar.

0021-9517/97 $25.00

Breck and Flanigen (25) first reported a linear correlationship between the unit cell volume and the chemical aluminum content of Na-Y-zeolites. With the advent of MAS NMR the framework Al concentration of Y-zeolites could be calculated with good accuracy using the ^{29}Si signal. Sohn *et al.* (26) have reported excellent linear correlationships between the NMR framework Al concentration, unit cell constant values and shifts of the IR frequencies of T-O vibrations. ^{27}Al signals can also be used to characterize framework and extra-framework aluminum. The latter could form different species such as polymeric moieties (27, 28), Al_2O_3 (29), and amorphous silica alumina (30). Consequently, the low symmetry environment of such extra-lattice aluminum originates large quadrupole interactions of the ^{27}Al nucleus with subsequent signal broadening, in some cases beyond detection. Recent measurements of very high quadrupole coupling constants (ca 15 MHz) of Al in Y-zeolites (31) further explain the difficulties to account for all the Al present in dealuminated zeolites.

An adequate characterization of lattice and extra-lattice aluminum in mordenite is less abundant and a correct quantification of these species is more difficult. The determination of framework Al by ^{29}Si MAS NMR is complicated by the presence of several kinds of SiOH groups. Although calculations are much more involved and subject to errors, some authors have selected this method (21, 32). Narrow ^{27}Al MAS NMR signals at 0 ppm and 54–55 ppm are assigned to Al^{VI} (extra-lattice) and Al^{IV} (lattice), respectively (33, 34). A broad band centered at ca 50 ppm is also shown in one of Meyers *et al.*'s spectra (33) and also assigned to amorphous aluminum oxides. These authors (33) have also explored the evolution of the cell constants with dealumination providing fresh data to compare with the original correlation shown by Olsson and Rollmann (35). Ha *et al.* (36), on the other hand, provide some information about the correlation between XRD and FTIR data.

In this work the dealumination that takes place during the acid treatment or under reaction conditions during the SCR of NO with methane, was monitored using ^{27}Al MAS NMR, ^{129}Xe NMR, XRD, and FTIR with the following purposes: (i) to have a reliable method to quantify framework aluminum; (ii) to achieve a better understanding of the physicochemical transformation that occurs during the deactivation process; (iii) to correlate such changes in the physicochemical properties with the catalytic activity.

2. EXPERIMENTAL

2.1. Catalysts Preparation

A commercial H-mordenite (Norton Zeolon 900H) with a $(Si/Al)_{Ch}$ ratio of 5.9, determined by chemical analysis, was the starting material. This is the same batch of mordenite used in a previous study (13). The dealumination was performed with HNO_3 at 90°C under the conditions shown in Table 1. The catalysts are named MH#F (or U), where M, mordenite; H, >99% in protonic form; #, Si/Al ratio from chemical analysis; F, fresh, and U, used.

TABLE 1

Catalysts Preparation and Chemical Structure of Acid Dealuminated H-Mordenites

Samples[a]	Dealumination conditions[b]		Unit cell[c]
	Time (h)	HNO_3 (*N*)	
MH5.9	Starting material		$H_{6.95}[(AlO_2)_{6.95}(SiO_2)_{41.05}]$
MH7.3	2	4	$H_{5.8}[(AlO_2)_{5.8}(SiO_2)_{42.2}]$
MH11.0	7	14	$H_{4.0}[(AlO_2)_{4.0}(SiO_2)_{44}]$
MH16.9	24	14	$H_{2.7}[(AlO_2)_{2.7}(SiO_2)_{45.3}]$

[a] Nomenclature of mordenite samples: M, mordenite; H, >99% in H-form; Si/Al ratio from chemical analysis.
[b] Acid leaching at 90°C.
[c] Unit cell from chemical analysis based on 48T unit/u.c.

2.2. ^{27}Al MAS NMR and ^{129}Xe NMR of Physisorbed Xenon

The NMR measurements were made using a Brucker MSL300 spectrometer. ^{27}Al MAS NMR spectra were taken at aluminum frequency of 78.15 MHz. Typically 10,000 to 25,000 transients were acquired at spinning frequencies ranging from 2.5 to 12 kHz, using a 4-mm diameter rotor with a double bearing system. The recycle delay was 0.25 s in each case and the resonance was observed in the absence of proton decoupling. The chemical shift was referenced with respect to a dilute solution of $Al(NO_3)_3$; $\pi/12$ pulses were used in all cases in order to make quantitative measurements. The spectral width was 1 MHz in order to detect and measure the intensity of the broad band component present in all spectra. The deadtime of the receiver was 2–4 times the dwell time.

A conventional BET system equipped with mechanical and oil diffusion pumps was used to measure the Xe adsorption isotherms at 20°C. Before adsorbing Xe the solid was evacuated overnight at 400°C.

^{129}Xe NMR spectra of physisorbed Xenon were taken at a frequency of 82.91 mHz. Between 1000 and 5000 scans were accumulated in order to obtain a good signal to noise ratio. The chemical shift was measured at Xe pressures between 10 and 600 mbar, and it was referred to the NMR signal of Xe in the gas phase extrapolated at zero pressure.

2.3. Infrared Spectra

They were taken using an FTIR Shimadzu DR-8001 instrument collecting 2000 spectra with a spectral resolution of 4 cm^{-1}. Self-supporting wafers of the samples (7–10 mg/cm^2) were mounted in a transportable infrared cell fitted with KBr optical windows. The samples were outgassed under vacuum at 400°C overnight. The

TABLE 2

Assignment of Lattice Vibrations in Mordenite

Band position (cm^{-1})[a]	Assignment	Ref.
570–600 (C)	T–O in 5-member rings	(37, 49)
650–660 (B)	Al–O belonging to alternating SiO_4 and AlO_4 tetrahedra and/or single 4-member rings	(36–38)
730–740 (A)	Isolated AlO_4 tetrahedra in 4-member rings	(36–38)

[a] A, B, and C are used to locate these bands in the spectra shown in Fig. 8.

measurements were taken under vacuum at room temperature. Table 2 shows the assignment of the T–O vibrations to different lattice configurations. The frequency shifts of the twin T–O signals at 572 cm^{-1} and 588 cm^{-1} (C) and the normalized intensity ratios A/C and B/C were used to characterize the dealumination process.

2.4. X-Ray Diffraction

The diffractograms were taken with a Shimadzu instrument XD-D1 model equipped with monochromator using Cu$K\alpha_1$ radiation. The spectra were obtained in continuous scanning mode at 0.5° (2θ) min^{-1} in the 15–35° (2θ) range. The X-ray tube was operated at 30 kV and 40 mA. The lattice parameters were determined using 10% by weight of Si as internal standard. For the calculations, Cohen's least square method was employed, using the following Miller's indexes reflections: [330], [150], [002], [411], [341], [431], [511], and [402].

2.5. Catalytic Measurements

The reaction was carried out using 0.5 g of catalyst placed in a fixed-bed flow reactor. This was a 12-mm i.d. tubular quartz reactor with an internal thermowell. The typical reacting mixture consisted of 1000 ppm of NO, 1000 ppm of CH_4, 10% of O_2, balanced at 1 atm with He (GHSV = 6500 h^{-1}). The composition of the reacting gases was analyzed with a Varian 3700 chromatograph with two columns, one packed with 5 A molecular sieve and the other with Chromosorb 102. The NO_x conversion was calculated from the N_2 production.

3. RESULTS

3.1. Catalytic Results

H-mordenites are active for the selective reduction of NO_x with CH_4 in the presence of excess oxygen. This is in agreement with results previously reported by Yogo *et al.* (12) and by our group (13). Figures 1A and B summarize the data obtained with H-mordenites having Si/Al ratios of 5.9, 7.3, 11.0, 16.9, showing a pronounced effect of the Al content on the catalytic activity.

When the samples were tested in a second cycle after being on stream for over 1 h at 650°C, a decrease of the catalytic activity was observed (Fig. 2). This decrease was neither intensified in successive cycles nor recovered by treatments in O_2 at 650°C. This irreversible deactivation may be related to a loss of lattice Al as a consequence of the high temperature and the presence of steam (produced by the reaction) in the reacting atmosphere. In order to verify this possibility, the measurement of the amounts of lattice and extra-lattice Al in the fresh and used samples was attempted.

3.2. ^{27}Al MAS NMR

Figure 3 shows the ^{27}Al MAS NMR spectrum of the fresh 5.9 sample obtained at 2.5 kHz spinning rate and a spectral bandwidth of 1 MHz. The spectrum exhibits three signals, one at 0 ppm corresponding to the extra-framework Al in octahedral coordination (Al^{VI}), another at 54 ppm assigned to undistorted framework Al sites (Al^{IV}), and a broad band associated with a combination of polymeric extra-lattice

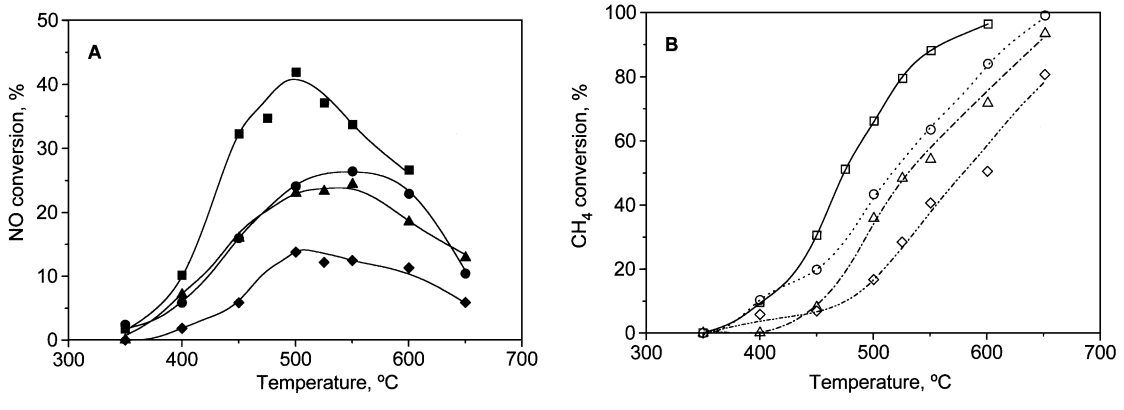

FIG. 1. Effect of the Si/Al ratio in the conversion of: (A) NO to N_2: ■, MHF5.9; ●, MHF7.3; ▲, MHF11.0; ◆, MHF16.9. (B) CH_4 to CO_2: □, MHF5.9; ○, MHF7.3; △, MHF11.0; ◇, MHF16.9.

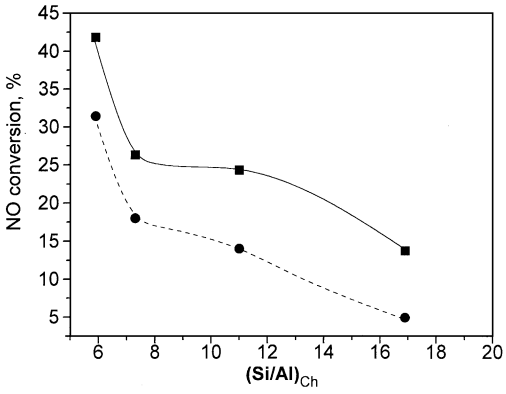

FIG. 2. Increasing chemical Si/Al ratio of H-mordenites decreases the maximum NO conversion over fresh (■) and used (●) samples.

aluminum species and distorted lattice sites. The latter two are probably due to the method of preparation of the protonic form. The same type of spectra was obtained for all fresh and used samples under study.

The presence of such a broad band made it more difficult to quantify the framework Al. In order to minimize dipolar coupling, chemical shift anisotropy, and first order quadrupole effects, ^{27}Al MAS NMR experiments at higher spinning rates were performed. The results obtained using the MH11.0 catalyst are shown in Fig. 4. The proportions of the different types of aluminum change with the spinning rate. At increasing rates, a decrease of the BB intensities, an increase of the Al^{IV} signal until reaching a plateau, and a slight increase of the signal corresponding to the Al^{VI} are observed (Fig. 4). The same experiments were performed with all the samples; similar results were obtained. Figure 5 shows the spectra corresponding to some of the samples under study (fresh and used) taken at 11.3 kHz. Note that, not even when dealumination was attained by means of an acid solution, was it possible to eliminate all the nonlattice aluminum. Similar results were reported by other authors (34, 39–41). Figure 5 also shows that both MHU7.3 and

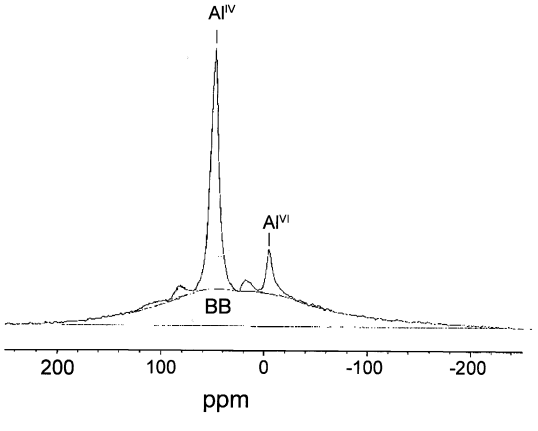

FIG. 3. ^{27}Al MAS NMR spectra of MHF5.9 acquired at 2.5 kHz and with a bandwidth of 1 MHz.

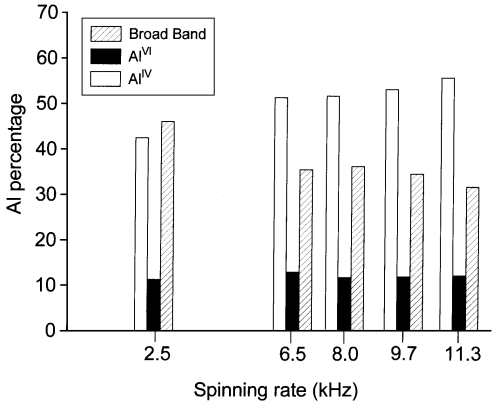

FIG. 4. Effect of the spinning rate on the signals of ^{27}Al MAS NMR. Sample: MHF11.0. Al percentage for each signal was determinated from integrated area ($Al^{VI} + Al^{IV} + BB = 100$).

MHU11.0, exhibit very sharp tall signals of Al^{VI} compared to the MHU16.9 sample. However, the area under these peaks does not increase so much if compared to fresh samples because they are very sharp.

Figure 6 summarizes the Al per unit cell (Al/u.c.) distribution for the fresh and used samples. The integrated intensity of the different signals obtained at the highest spinning rate was plotted. However, when a Na-mordenite sample (Valfor CP500) which only has framework Al, was used as the external standard to quantify the Al signals, it was possible to account for only 70–80% of the total Al in all the samples.

Comparing the fresh and used samples, Fig. 6 shows a significant increase in the BB after use and the opposite effect in the Al^{IV} signal, while the small Al^{VI} signal slightly increases after use, a trend observed for all the samples under study. An exception to this behavior is MHU7.3 which shows a significant increase in intensity of the octahedral signal.

At this point special attention must be given to the way in which Al is being quantified. In fact, the number of framework Al per unit cell is not always the same, depending on whether the broad band is considered or not. In principle,

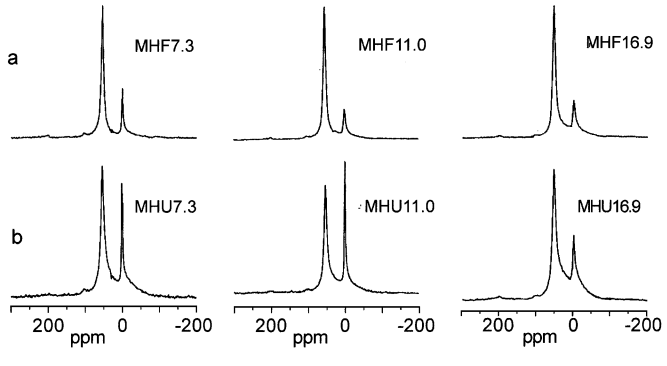

FIG. 5. ^{27}Al MAS NMR spectra measured at 11.3 kHz: (a) fresh samples; (b) used samples.

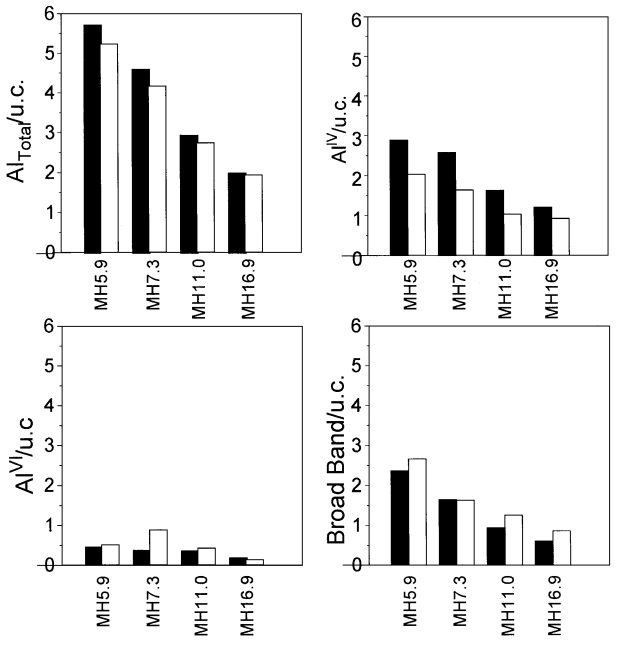

FIG. 6. ^{27}Al MAS NMR aluminum distribution obtained at 11.3 kHz: ▬, fresh samples; ▭, used samples. Al/u.c. was determined from integrated area taking as reference Na-mordenite (Valfor CP500).

we used three models to process the data obtained from the ^{27}Al MAS NMR spectra.

Model 1. Frequently used in the literature, it assumes that the Al extracted from the lattice only forms Al species with octahedral coordination. Thus, the values of Al_{total} $(Si/Al)_f$ framework ratio, and Al/u.c. are obtained from Eqs. [1], [2], and [3], respectively:

$$Al_{total} = Al^{IV} + Al^{VI} \quad [1]$$

$$(Si/Al)_f = (Si/Al)_{ch} \cdot \left(Al_{total}/Al^{IV}\right) \quad [2]$$

$$Al/u.c. = 48/[(Si/Al)_f + 1]. \quad [3]$$

Model 2. The broad band is included in the Al balance, i.e., the Al extracted from the lattice from Al^{VI} moieties and polymeric species of low crystallinity, the latter being responsible for the BB. The difference between this model and the former one consists in the way of quantifying the Al_{total}. In this case, Al_{total} is given by Eq. [4],

$$Al_{total} = Al^{IV} + Al^{VI} + BB. \quad [4]$$

The $(Si/Al)_f$ ratio and Al/u.c. are obtained from Eqs. [2] and [3].

It is implicitly assumed in this model that the Al visible by NMR represents the total aluminum present in the samples.

Model 3. Estimation of the amount of Al/u.c. was carried out by measuring only the intensity of the 54 ppm signal corresponding to Al^{IV}, referred to Valfor CP500. Therefore, only the Al seen by NMR are quantified in this case.

TABLE 3

Framework Al Concentration Calculated from ^{27}Al MAS NMR Measurements[a]

Samples	Chemical[b]	Model 1[c]	Model 2[d]	Model 3[e]
MHF5.9	6.95	6.11	3.52	2.93
MHU5.9	6.95	5.70	2.98	2.06
MHF7.3	5.78	5.12	3.42	2.61
MHU7.3	5.78	3.92	2.46	1.66
MHF11.0	4.00	3.23	2.31	1.66
MHU11.0	4.00	2.83	1.60	1.05
MHF16.9	2.68	2.34	1.66	1.23
MHU16.9	2.68	2.34	1.32	0.94

[a] Al per unit cell.
[b] From chemical analysis.
[c] Al_{total}, $(Si/Al)_f$, and Al/u.c. are obtained from Eqs. [1], [2], and [3], respectively (see text).
[d] The $(Si/Al)_f$ ratio and Al/u.c. are obtained from Eqs. [2] and [3] and the Al_{total} is calculated from Eq. [4].
[e] The estimation of the amount of Al/u.c. was carried out by measuring only the intensity of the 54 ppm signal corresponding to Al^{IV}, referred to Valfor CP500.

Table 3 presents the results obtained from the calculation of structural aluminum, according to the three models proposed and compared with that obtained by chemical analysis. The Al/u.c. values calculated from Model 1 are close to those obtained by chemical analysis. This model overestimates the amount of lattice Al, since the Al extracted from the framework form species appearing in the BB, rather than species with octahedral coordination (Fig. 3). Models 2 and 3 yield better estimations of framework aluminum concentration by taking into account the BB contribution. The latter seems to be the most accurate for it is independent of the invisible extra-lattice aluminum. Further evidence of this was obtained when the turnover frequency of the NO disappearance was plotted against the Al framework per gram calculated according to model 3. Figure 7 shows the results at two temperatures. In all cases TON was almost

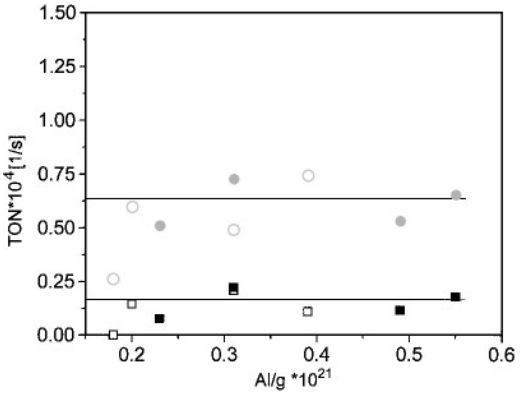

FIG. 7. Effect of framework aluminum on NO disappearance turnover number. Full symbols: Fresh samples. Open symbols: Used samples. ■, □, at 400°C; ●, ○, at 525°C.

constant except for MHU 16.9 (vide infra). The values of the turnover number were obtained from the equation

$$TON = (GHSV \cdot [NO]^{\circ} \cdot X_{NO})/(\delta \cdot Al^{IV}/g \cdot 3600); \quad [s^{-1}],$$

where $[NO]^{\circ}$ represents the concentration of NO in the feed (molecules/cm^3), X_{NO} is the NO conversion, and δ is the bed density.

3.3. FTIR

It has been reported that IR frequencies of T–O vibrations of the zeolite structure shift towards high frequencies as the Si/Al framework ratio increases (26, 37, 38). Consequently, in order to obtain additional information related to the dealumination process and to confirm the ^{27}Al MAS NMR data, IR spectra for the fresh and used samples in the region between 400 and 1100 cm^{-1} were obtained. Figure 8 presents the IR spectra obtained for the fresh and used selected samples with the highest and the smallest Si/Al ratios, respectively. The bands associated with the structural tetrahedra (See bands assignments in Table 2) are shifted to higher wavenumbers as the Al content decreases. Besides, the signals appearing at 650 and 730 cm^{-1} decrease in intensity as the dealumination progresses.

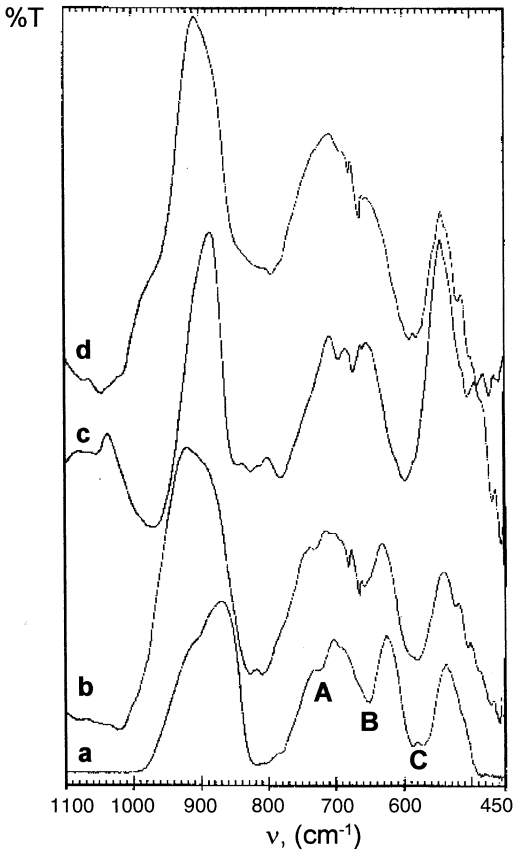

FIG. 8. Evolution of the FTIR spectra (T–O region) of H-mordenites with varying Si/Al ratios: (a) MHF5.9; (b) MHU5.9; (c) MHF16.9; (d) MHU16.9. For assignments signals A, B, and C see Table 2.

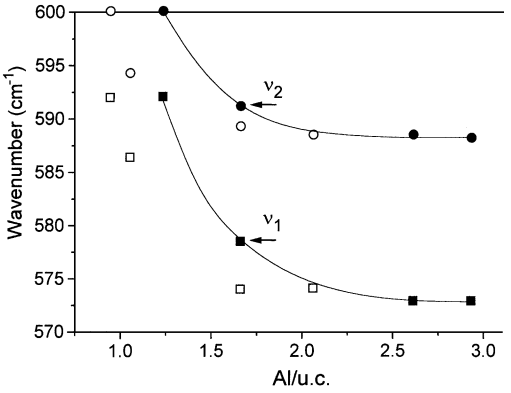

FIG. 9. Dealumination affects the frequencies of T–O vibrations in 5-member rings. Full symbols: Fresh samples. Open symbols: Used samples. ■, □: ν_1 (572–592 cm^{-1}); ●, ○: ν_2 (588–600 cm^{-1}).

As shown in Fig. 9 the frequency shifts in the bands at approximately 572 cm^{-1} (ν_1) and 588 cm^{-1} (ν_2) do not change linearly with the Al/u.c. content, as was the case in Y-Zeolites (26). Table 4 presents the normalized transmittance ratios A/C and B/C obtained for fresh and used samples. It was observed (not shown) that the normalized transmittance ratios A/C and B/C for fresh samples linearly correlate with the Al^{IV} content determined by ^{27}Al MAS NMR. However, the used samples do not fit well this correlation. This can be due probably to the fact that the amorphous aluminum left inside the mordenite channels may interfere with the aluminum in the structure, thus provoking the broadening of some bands.

3.4. XRD

The cell parameters can also give information related with the Al framework content (33). With this purpose and in order to know how dealumination (either by acid

TABLE 4

Effect of Lattice Aluminum Concentration upon the Intensity of the IR Bands

Catalysts	Al/u.c.[a]	Normalized IR intensity ratios A/C[b]	B/C[c]
MHF5.9	2.93	0.107	0.702
MHU5.9	2.06	0.105	0.671
MHF7.3	2.61	0.085	0.523
MHU7.3	1.66	0.062	0.657
MHF11.0	1.66	0.03	0.24
MHU11.0	1.05	0.078	0.387
MHF16.9	1.23	0.019	0.11
MHU16.9	0.94	0.005	0.235

[a] Calculated using model 3.

[b] A/C: Intensity of the 730 cm^{-1} band referred to the 572–600 cm^{-1} signal (see Fig. 8).

[c] B/C: Intensity of the 650 cm^{-1} band referred to the 572–600 cm^{-1} signal (see Fig. 8).

TABLE 5

Effect of Si/Al Ratio on Crystallinity and Cell Constants[a]

Samples	Crystallinity[b]	Cell constants (Å) a	b	c	Cell volume (Å^3)
MHF5.9	100.0	18.17	20.38	7.47	2766
MHU5.9	99.3	18.17	20.38	7.47	2766
MHF7.3	98.9	18.09	20.28	7.45	2733
MHU7.3	94.6	18.09	20.32	7.46	2742
MHF11.0	94.8	18.07	20.22	7.43	2715
MHU11.0	83.2	18.04	20.19	7.42	2703
MHF16.9	93.2	18.03	20.23	7.44	2714
MHU16.9	70.1	17.71	19.93	7.46	2633

[a] Cohen's least square method was employed, using the following Miller's indexes: [330], [150], [002], [411], [341], [431], [511], and [402].

[b] Degree of crystallinity calculated from $K = 100/[1 + k(I_A/I_C)]$, where $k = 1$ and I_A, I_C are the intensities of the amorphous and crystalline phases, respectively. Values referred to the MH5.9 sample.

TABLE 6

Textural Features Derived from the N_2 Adsorption Isotherms

Samples	S_{BET}[a] [m^2/g]	S^t_{micro}[b] [m^2/g]	S^t_{meso}[c] [m^2/g]	S_{ext}[d] [m^2/g]	V_{micro}[e] [cm^3/g]
MHF5.9	436	352	84	8.9	0.221
MHU5.9	405	315	90	15.6	0.205
MHF7.3	417	326	91	14.2	0.207
MHU7.3	333	223	110	20.0	0.165
MHF11.0	405	303	101	16.1	0.203
MHU11.0	321	198	123	18.1	0.159
MHF16.9	431	290	141	22.8	0.215
MHU16.9	400	278	122	20.4	0.202

[a] BET surface area.

[b,c] Surface of micro and mesopores calculated by the *t* method.

[d] External surface calculated by the Remy and Poncelet method.

[e] Micropore volume calculated by the D-R method considering only the N_2 adsorbed in the micropores.

or hydrothermal treatment under reaction conditions) can change the crystallinity of the mordenites, an XRD systematic study was performed over fresh and used samples. Crystallinity and the cell parameters of the mordenites employed are reported in Table 5. The values obtained are comparable with others in the literature (32, 33). Neither the acid nor the hydrothermal treatment in the reaction stream provokes a significant change in crystallinity. The structure disruption in the samples studied was less than 5% with the exception of samples MHF11 and MHF16.9, where after 1 h under reaction stream at 650°C, 16.8% and 29.9% crystallinity losses were detected, respectively.

For the fresh samples, the *a* constant steadily decreases with diminishing Al content, while constants *b* and *c* follow this trend until Al/u.c. $\cong 2$. For lower Al concentrations, constants *b* and *c* begin a gradual expansion. The net result is a steady decrease of the cell volume. The reaction stream had no significant effect on the unit cell constants for the used samples, with the exception of MHU16.9, where a cell shrinkage was observed. This could be due to the ill-defined XRD patterns of this sample (vide supra). In any case, when comparing fresh and used samples, this method is not sensitive enough to detect the dealumination that occurs in H-mordenites after being on stream for 1 h at 650°C.

3.5. N_2 Adsorption

Specific surface area and micropore volume were calculated for each sample from the N_2 adsorption isotherms. With this object, BET, the *t* method and the calculation procedure proposed by Remy and Poncelet (42) were applied. The S_{BET} and V_{micro} values shown in Table 6 indicate that the acid dealumination process does not significantly modify the adsorption capacity of H-mordenites. However, mesopores are formed as the dealumination progresses, thus provoking an increase of the external surface (S_{ext}). By comparing fresh and used catalysts, some changes occur in the solid structures after reaction at 650°C. The decrease in the micropore volume is accompanied by an increase in the external surface, probably also due to mesopore formation under reaction conditions. The used MH16.9 catalyst is again an exception to this trend.

3.6. ^{129}Xe NMR of Physisorbed Xenon

The N_2 adsorption revealed that some pore blockage may occur due to dealumination. In an attempt to throw light on this process, ^{129}Xe NMR experiments were done on fresh and used samples.

Figure 10 shows the Xe adsorption isotherms for the different dealuminated samples of H-mordenites. The adsorption capacity of the samples decreases as the degree of dealumination increases. Similar results were obtained with used samples. ^{129}Xe NMR spectra of physisorbed Xenon for the different H-mordenites are shown in Fig. 11 for a pressure of approximately 200 mbar and 293 K. The

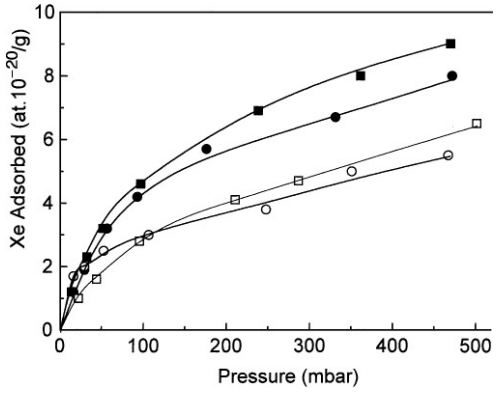

FIG. 10. Adsorption isotherms of Xe on H-mordenites at 20°C: ■, MHF5.9; ●, MHF7.3; □, MHF11.0; ○, MHF16.9.

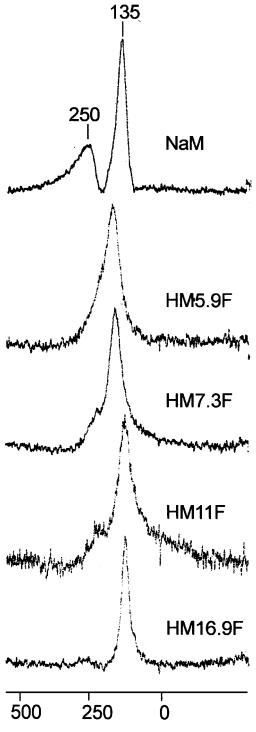

FIG. 11. ^{129}Xe NMR of physisorbed Xenon on mordenites.

spectrum corresponding to the Na-mordenite sample is also shown as reference. The catalyst with Si/Al = 5.9 shows a single peak due to the well-known coalescence effect, indicating the Xenon free exchange between the main channels and the side pockets. As the dealumination degree increases, the peak corresponding to the side pockets starts appearing again, even though it is smaller, if compared to the Na-mordenite. These results suggest that nonframework Al may obstruct the access to the mordenite side-pocket as Na does. The same results were observed when fresh and used samples were compared (Fig. 12).

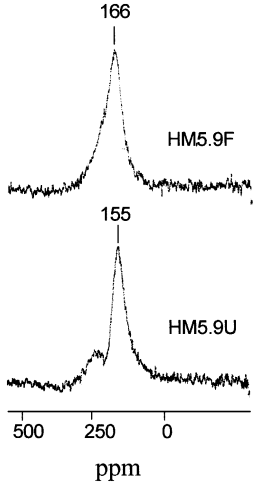

FIG. 12. ^{129}Xe NMR of physisorbed Xenon on fresh and used MH5.9.

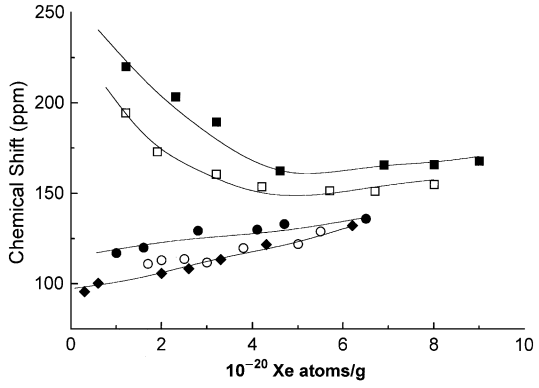

FIG. 13. ^{129}Xe chemical shift at different concentrations of adsorbed Xenon on fresh catalysts: ■, MHF5.9; □, MHF7.3; ●, MHF11.0; ○, MHF16.9; ◆, Na-mordenite.

Further evidence of such behavior was obtained when the chemical shift (ppm) of the main peak was plotted against the different adsorbed amounts of Xenon in Fig. 13. The curves corresponding to catalysts with Si/Al 5.9 and 7.3 present a minimum at approximately 6×10^{20} atoms of Xenon per gram, the form of the curve being qualitatively similar to that reported for H-Zeolon (33). Instead, for higher degrees of dealumination (11.0 and 16.9) results become progressively closer to those corresponding to the Na-mordenite reference sample.

4. DISCUSSION

The catalytic activity for the reduction of NO with methane on fresh H-mordenites increases with the aluminum concentration (Fig. 1). Besides, these catalysts deactivate after being on stream for 1 h at 650°C (Fig. 2). The decrease of the framework tetrahedral aluminum (Fig. 6 and Table 3) and the constancy of the turnover frequency of NO disappearance with the amount of tetrahedral aluminum (Fig. 7) strongly suggests that the main cause of deactivation is the dealumination that occurs during reaction at high temperature. This process may be accompanied by a change of strong acid site concentration (13), some structure disruption, and micropore blockage (Tables 5 and 6 and Figs. 10–12). It is well known that both acid and thermal dealumination of H-mordenites (44, 45), leaves Al^{VI} species and polymeric residues of low crystallinity inside the pore structure. The latter, which is more pronounced in the steam-dealumination process (45), gives rise to a broad band in the ^{27}Al MAS NMR spectrum from which the much sharper tetrahedral and octahedral aluminum signals emerge (Fig. 3). In view of this and taking into account ^{27}Al MAS NMR results (Figs. 5 and 6), it could be suggested that the tetrahedral aluminum removed from the zeolite framework during reaction mainly forms polymeric species. This would confirm that steam-dealumination

occurs on stream when the temperature is 650°C or higher, due to water formed by the reaction. A similar dealumination was reported by Armor and Farris (46) in the case of Cu-ZSM-5, but after exposure to 2% H_2O at 750°C. Yan *et al.* (21) also found some dealumination for Cu-ZSM-5 after the wet SCR of NO with propene at 400°C and by Grinsted *et al.* (20) for the same type of material after aging in a He stream with 10% H_2O at 410°C.

The results of Fig. 5 also show that the Al^{VI} signal already present in the fresh samples becomes sharper in the used catalysts but the integrated area slightly increases in all the samples (Figs. 5 and 6) with the exception of MHU7.3 which shows a significant increase in intensity. The same behavior was reported by O'Donovan *et al.* (47). They found that the acid washing of the previously steamed dealuminated mordenite changed the shape of the octahedral peak, becoming similar to that appearing in acid-washed mordenite.

In our case, the increase in the octahedral symmetry which goes along with the catalyst deactivation may be due to the formation of $[Al(H_2O)_6]^{+3}$. These species are usually observed after acid treatments (34) and present high symmetry. The reaction medium inside the zeolite crystals may be strongly acidic. In effect, NO_3^- species were reported to be present on H-ZSM-5 when NO and O_2 were co-adsorbed (48). Additionally, if this occurs the aluminum moieties formed may move to more accessible positions near the pore mouths (45). Consistent with this hypothesis is the fact that the two used catalysts, MHU7.3 and 11.0, which show the sharpest signals, are also those exhibiting the largest decrease in pore volume (Table 6).

The Xe adsorption isotherms for the different dealuminated samples show that the adsorption capacity of the solids decreases as the degree of dealumination increases (Fig. 10). ^{129}Xe NMR spectra indicates that the extra-lattice aluminum species can be located either in the main channels or obstructing the access to the side-pockets. The latter species may contribute to hinder the free diffusion of reactants inside the zeolite framework. However, it seems that the nonlattice aluminum, whatever their location or type, do not play any important role in the reaction mechanism as suggested by the results in Fig. 7.

In a previous communication (13) we have suggested that the strength of the acid sites may play a role in the SCR system. This was based upon the observed decrease in high temperature ammonia adsorption after the catalyst had been 1 h on stream at 650°C. The present results, particularly the constancy of the TON (Fig. 7), do not lend support to this hypothesis. With the present data no definite conclusion can be reached concerning the role of Bronsted acid sites in this system.

IR results obtained in acid-washed dealuminated mordenites (Fig. 8) show that the lattice Al extraction produces a decrease in the intensity of the bands at 650 and 730 cm^{-1}. Note that the Al located at 5-member rings (associated with the twin bands ca 572 and 588 cm^{-1}) are stable in the samples with high aluminum content. Nevertheless, the band shift sharply increases for the more dealuminated samples (Fig. 9), thus indicating that the Al extraction selectively occurs at $T_{1,2}$ positions in these samples. Used samples also fit the same correlation mainly in samples with high Al content. The linear decrease in the intensity of the signals at 650 and 730 cm^{-1} with diminishing framework Al content (Table 4) would be pointing out that the acid leaching also extracts the Al located at 4-member rings ($T_{3,4}$). These results are in general agreement with those reported by van Geem *et al.* (38). The intersection with the axis at intensity zero, at about 35% of Al^{IV} (ca 1 Al per unit cell) would indicate that the remaining Al^{IV} are not connected with the isolated 4-member rings. van Geem *et al.* (38) found that such intersection occurs at about 65%. The discrepancy could be due to: (i) the different types of mordenites employed in the two studies; (ii) the IR band used to normalize the intensity of the signals at 650 and 750 cm^{-1}. While they employed a signal at 450 cm^{-1} assigned to bending vibrations of Al–O and Si–O, in our case the reference was the band at 570–600 cm^{-1} due to the Al–O vibrations in the 5-member rings. From the results in Fig. 8 and Table 4 it could be concluded that the Al are extracted at random both from $T_{1,2}$ (5-member rings) and $T_{3,4}$ framework positions (4-member rings). Our results also confirm the random Al distribution in all the sites of the mordenite structure reported by van Geem *et al.* (38). This is not in agreement with what was proposed by other authors (35, 41) who concluded that the most stable positions are the $T_{3,4}$ located at 4-member rings. The dealumination suffered by H-mordenite under reaction conditions follows the same general trend. However, the decrease of the signal at 730 cm^{-1} do not fit very well with the correlation obtained in the acid-washed sample (Table 4). This could be attributed to the difficulty in quantifying the 730 cm^{-1} band integrated area (Fig. 8). Our results show that notwithstanding the high extent of dealumination reached in the samples under study, all of them maintain a high degree of crystallinity (Table 5) and similar adsorption capacity, which may indicate that, although Al was extracted from $T_{3,4}$, no structure collapse occurred.

The ^{27}Al MAS NMR results (Figs. 3–5 and Table 3) show that care must be exercised when quantifying the Al present in the dealuminated H-mordenites. This is particularly true when an accurate estimate of nonframework aluminum is needed. Even by spinning the samples at 11.3 kHz only 70–80% of the total Al was seen. This is at variance with the conclusion reached by Klinowski and co-workers and O'Donovan *et al.* (34, 47) who claimed that they were able to account for all the aluminum present in H-mordenites at ca 12 kHz and 2.5 kHz, respectively. Such discrepancy could be attributed to the fact that the samples used in these studies contained low percentages of polymeric extra

lattice aluminum (34, 47). We do agree with Klinowski and co-workers (34) that ^{29}Si MAS NMR can lead to reliable quantitative data when this technique is applied to mordenite samples with low content of silanol groups. In the dealuminated samples the ^{29}Si peak at ca −106 ppm may arise from both Si(1Al) and the Si–OH sites generated by extraction of Al from the framework. In our dealuminated samples, the lattice Al could not be determined through this method since only a broad peak at −113 ppm with a shoulder at ca −106 ppm was obtained. In this particular study the best quantitative estimation of framework aluminum was obtained from the integrated intensity of the Al^{IV} signal (Model 3, Table 3). The 572 and 588 cm^{-1} IR bands shift (Fig. 9) also correlate with the Al content per unit cell obtained from Model 3. Consequently, this correlation could also be used to quantify the lattice aluminum content.

5. CONCLUSIONS

Our results show that:

i. The active sites for the selective reduction of NO with methane on H-mordenite are strongly related to Al^{IV} (lattice aluminum). Nonlattice, polymeric species, only could contribute to hinder the free diffusion of reactants inside the mordenite framework (Fig. 7).

ii. The main cause of the H-mordenite deactivation is the dealumination occurring upon reaction at 650°C (Figs. 5 and 6), simultaneously with some structure disruption and pore blocking (Table 6 and Figs. 12 and 13).

iii. The extra-lattice aluminum forms very symmetrical octahedral species and to a larger extent polymeric moieties (Figs. 3 and 5). The dealumination that takes place resembles the one occurring during steaming and acid-washing (34, 47).

iv. ^{129}Xe NMR confirms that extra-lattice aluminum is reaccommodated during the chemical reaction thus partially obstructing the Xe free exchange between the main channels and the side pocket (Fig. 12). This restriction could contribute to the loss of activity of the catalyst.

v. Care should be taken in the quantification of extra-lattice Al due to the high quadrupole effects that cannot be completely eliminated, even at high spinning rates, ca 12 kHz (Figs. 4 and 5).

vi. The intensity of the Al^{IV} signal yields the most reliable data to quantify the framework Al of highly dealuminated H-mordenites with abundant extra-lattice Al containing polymeric oxides.

vii. IR spectral data yield valuable information to complement the MAS NMR data. They help to better characterize the dealumination mechanism (Fig. 8, Table 6). Note the higher tendency of T1 and T2 sites to undergo dealumination. The 572 and 588 cm^{-1} IR bands shift can also be employed to quantify lattice aluminum (Fig. 9).

ACKNOWLEDGMENTS

This work was performed under European Union Contract CI1*CT93-0090. Thanks are given to CONICET and UNL for partial support, to the Japan International Cooperation Agency for the donation of the IR spectrometer, X-ray diffractometer, and sorptometer to the National Catalysis Center, and to Elsa Grimaldi for the English edition.

REFERENCES

1. Iwamoto, M., "Proceedings, Meeting of Catalytic Technology for Removal of Nitrogen Monoxide, Tokyo, 1990," p. 17.
2. Held, W., Koning, A., Ritcher, T., and Puppe, L., SAE Paper 900496, 1990.
3. Truex, T. S., Searle, R. A., and Sun, D. C., *Plat. Met. Rev.* **36**, 1 (1992).
4. Li, Y., and Armor, J. N., U.S. Patent 5,149,512 (1992).
5. Petunchi, J. O., Sill, G. A., and Hall, W. K., *Appl. Catal. B* **2**, 303 (1993).
6. Li, Y., and Armor, J. N., *J. Catal.* **150**, 376 (1994).
7. Lukyanov, D. B., Lombardo, E. A., d'Itri, J. L., Sill, G., and Hall, W. K., *J. Catal.* **163**, 447 (1996).
8. Burch, R., and Scire, S., *Appl. Catal. B* **3**, 295 (1994).
9. Kharas, K. C. C., Robota, H. J., and Liu, D. J., *Appl. Catal. B* **2**, 225 (1993).
10. Li, Y., and Armor, J. N., *Appl. Catal. B* **2**, 239 (1993).
11. Hamada, H., Kintaichi, Y., Sasaki, M., and Ito, T., *Appl. Catal.* **64**, L1 (1990).
12. Yogo, K., Umeno, M., Watanabe, H., and Kikuchi, E., *Catal. Lett.* **19**, 131 (1993).
13. Lezcano, M., Ribotta, A., Miró, E., Lombardo, E., Petunchi, J., Moreaux, C., and Dereppe, J. M., "Studies in Surface Science and Catal.," Vol. 101 B, p. 971, Elsevier, Baltimore, 1996.
14. Lukyanov, D. B., d'Itri, J. L., Sill, G., and Hall, W. K., "Studies in Surface Science and Catal.," Vol. 101 A, p. 651, Elsevier, Baltimore, 1996.
15. Li, Y., and Armor, J. N., *Appl. Catal. B* **1**, L31 (1992).
16. Inui, T., Iwamoto, S., Matsuba, K., Tanaka, Y., and Yoshida, T., *Catal. Today* **26**, 23 (1995).
17. Vassallo, J., Miró, E., and Petunchi, J., *Appl. Catal. B* **7**, 65 (1995).
18. Witzel, F., Sill, G. A., and Hall, K. W., *J. Catal.* **149**, 229 (1994).
19. Lukyanov, D. B., Sill, G., d'Itri, J., and Hall, W. K., *J. Catal.* **153**, 265 (1995).
20. Grinsted, R. A., Zhen., H. W., Montreuil, C., Rokosz, M. J., and Shelef, M., *Zeolites* **13**, 602 (1993).
21. Yan, J. Y., Lei, G. D., Sachtler, W. M. H., and Kung, H. H., *J. Catal.* **161**, 43 (1996).
22. Petunchi, J., and Hall, W. K., *Appl. Catal. B* **3**, 239 (1994).
23. Kucherov, A. V., Gerlock, J. L., Jen, H, W., and Shelef, M., *J. Phys. Chem.* **98**, 4892 (1994).
24. Li, Y., and Armor, J. N., *J. Catal.* **145**, 1 (1994).
25. Breck, D. W., and Flanigen, D. M., "Molecular Sieves," p. 47, Soc. Chem. Indus., London, 1968.
26. Sohn, J. R., DeCanio, S. J., Lunsford, J. H., and O'Donnell, D. J., *Zeolites* **6**, 225 (1986).
27. Klinowski, J., Fyfe, C., and Globbi, G. J., *J. Chem. Soc. Faraday Trans.* **81**, 3003 (1985).
28. Rocha, J., and Klinowski, J., *Microporous Mat.* **1**, 70 (1992).
29. Lohse, U., and Mildebrath, M., *Z. Anorg. Allg. Chem.* **476**, 126 (1981).
30. Sanz, J., Fornés, V., and Corma, A., *J. Chem. Soc. Faraday Trans.* **84**, 3113 (1988).
31. Grey, C. P., and Vega, A. J., *J. Am. Chem. Soc.* **117**, 8232 (1995).
32. Hong, Y., Gruver, V., and Fripiat, J. J., *J. Catal.* **150**, 421 (1994).
33. Meyers, B. L., Fleisch, T. H., Ray, G. J., Miller, J. T., and Hall, J. B., *J. Catal.* **110**, 82 (1988).

34. Barras, J., Klinowski, J., and McComb, D. W., *J. Chem. Soc. Faraday Trans.* **90**, 3719 (1994).
35. Olsson, R. W., and Rollmann, L. D., *Inorg. Chem.* **16**, 651 (1977).
36. Ha, B. B. H., Guidot, J., and Barthomeuf, D., *J. Chem. Soc. Faraday Trans.* **75**, 1245 (1979).
37. Coudurier, G., Naccache, C., and Védrine, J. C., *J. Chem. Soc., Chem. Commun.*, 1413 (1982).
38. van Geem, P. C., Scholk, K. F. M. G. J., van der Velden, G. P. M., and Veeman, W. S., *J. Phys. Chem.* **92**, 1585 (1988).
39. Fernandes, L. D., Bartl, P. E., Fontes Monteiro, L., Gusmão da Silva, J., Cabral de Menezes, S., and Cardoso, M. J. B., *Zeolites* **14**, 533 (1994).
40. van Niekerk, M. J., Fletcher, J. C. Q., and O'Connor, C. T., *J. Catal.* **138**, 150 (1992).
41. Boudart, P., Nagy, J. B., Debras, G., Gabelica, Z., and Jacobs, P. A., *J. Phys. Chem.* **90**, 5183 (1986).
42. Remy, M. J., and Poncelet, G., *J. Phys. Chem.* **99**, 773 (1995).
43. Springuel-Huet, M. A., and Fraissard, J. P., *Zeolites* **12**, 841 (1992).
44. Stach, H., Jänchen, J., Jerschkewitz, H-G., Lohse, U., Parlitz, B., and Zibrowius, B., *J. Phys. Chem.* **96**, 8473 (1992).
45. Miller, J. T., Hopkins, P. D., Meyers, B. L., Ray, G. J., Roginski, R. T., Zajac, G. W., and Rosenbaum, N. H., *J. Catal.* **138**, 115 (1992).
46. Armor, J. N., and Farris, T. S., *Appl. Catal. B* **4**, L11 (1994).
47. O'Donovan, A. W., O'Connor, C. T., and Koch, K. R., *Microporous Mat.* **5**, 185 (1995).
48. Hoost, T. E., Laframboise, K. A., and Otto, K., *Appl. Catal. B* **7**, 79 (1995).